Asymptotic-Preserving Particle-In-Cell method for the Vlasov-Poisson system near quasineutrality

Pierre Degond, Fabrice Deluzet, Laurent Navoret, An-Bang Sun, Marie-Hélène Vignal

Asymptotic-Preserving Particle-In-Cell method for the Vlasov-Poisson system near quasineutrality

Pierre Degond[1], Fabrice Deluzet[2], Laurent Navoret[3], An-Bang Sun[4], Marie-Hélène Vignal[5]

[1]Université de Toulouse; UPS, INSA, UT1, UTM; Institut de Mathématiques de Toulouse; F-31062 Toulouse, France and CNRS; Institut de Mathématiques de Toulouse UMR 5219; F-31062 Toulouse, France.
(pierre.degond@math.univ-toulouse.fr).

[2]Université de Toulouse; UPS, INSA, UT1, UTM; Institut de Mathématiques de Toulouse; F-31062 Toulouse, France and CNRS; Institut de Mathématiques de Toulouse UMR 5219; F-31062 Toulouse, France.
(fabrice.deluzet@math.univ-toulouse.fr).

[3]Université de Toulouse; UPS, INSA, UT1, UTM; Institut de Mathématiques de Toulouse; F-31062 Toulouse, France and CNRS; Institut de Mathématiques de Toulouse UMR 5219; F-31062 Toulouse, France.
(laurent.navoret@math.univ-toulouse.fr).

[4]Université de Toulouse; UPS, INSA, UT1, UTM; Institut de Mathématiques de Toulouse; F-31062 Toulouse, France and CNRS; Institut de Mathématiques de Toulouse UMR 5219; F-31062 Toulouse, France.
(an-bang.sun@math.univ-toulouse.fr)
and The college of astronautics, Northwestern Polytechnical University, No.127 Youyi Xilu, Xi'an, China (absun1984@hotmail.com).

[5]Université de Toulouse; UPS, INSA, UT1, UTM; Institut de Mathématiques de Toulouse; F-31062 Toulouse, France and CNRS; Institut de Mathématiques de Toulouse UMR 5219; F-31062 Toulouse, France.
(mhvignal@math.univ-toulouse.fr).

abstract This paper deals with the numerical resolution of the Vlasov-Poisson system in a nearly quasineutral regime by Particle-In-Cell (PIC) methods. In this regime, classical PIC methods are subject to stability constraints on the time and space steps related to the small Debye length and

large plasma frequency. Here, we propose an "Asymptotic-Preserving" PIC scheme which is not subject to these limitations. Additionally, when the plasma period and Debye length are small compared to the time and space steps, this method provides a consistent PIC discretization of the quasineutral Vlasov equation. We perform several one-dimensional numerical experiments which provide a solid validation of the method and its underlying concepts.

keywords : Vlasov-Poisson, quasineutral limit, asymptotic preserving scheme, plasma, Debye length

AMS classification: 82D10, 76W05, 76X05, 76N10, 76N20, 76L05

1 Introduction

The impact of plasmas and more generally, charged-particle fluids on the human environment is constantly increasing, due to their importance in such domains as industrial processes, energy, lighting, air or water cleaning, etc. Because of the large variety of physical situations and the complex multiscale character of most plasma phenomena, the numerical simulation of plasmas still represents an important challenge for the scientific community. Roughly speaking, according to the physical context, two large classes of mathematical models can be used: fluid models and kinetic ones. This paper is concerned with collisionless plasmas for which a kinetic description is required.
The basic kinetic model for plasma simulations is the Vlasov equation, coupled with the electromagnetic field equations. The Vlasov equation is posed on a 6-dimensional phase-space (3 space dimensions and 3 velocity dimensions) plus time. For this reason, particle methods have been preferred to grid-based (eulerian) methods, as they allow a coarse, yet sufficiently precise, description of the phase space. In Particle-In-Cell methods, the coupling between the particles and the field is implemented through the introduction of a space grid. Charge and current densities are assigned from the particles to the grid. Then, the fields are computed using finite difference methods on the grid and then, interpolated back to the positions of the particles. We refer to the two celebrated books [3, 27] for an overview of these methods. Recently, grid-based eulerian simulations have received a great deal attention [1, 6, 16, 17, 18, 38, 40] but particle methods are still the number-one method used for the numerical simulation of plasma kinetic models. The convergence

of PIC methods has been mathematically investigated in [9, 19].
One of the very basic but very important problem in plasma simulations is the handling of quasineutrality. Indeed, the electrostatic force tends to restore the local charge neutrality of the plasma. The Debye length and plasma periods [7, 30] set the typical space and time scales at which this restoring force acts. The Debye length measures the typical scale of charge unbalances in the plasma whereas the electron plasma period characterizes the oscillation period of the particles when a departure to quasineutrality occurs. Usually, both these space and time scales are very short compared to the typical scales of the phenomena under investigation. In such situation, the plasma is locally quasineutral. These very short time scales make numerical simulations very time consuming. Indeed, standard explicit PIC methods require a stability condition which guarantees that the space and time steps are smaller than the Debye length and electron plasma period.
Lots of efforts have been devoted to the search for implicit PIC schemes which would be free of such constraints. There are basically two classes of implicit PIC methods : the direct implicit method [8, 31] and the implicit moment method [33, 34]. In the direct implicit method, an implicit algorithm for the advancement of the particles is introduced. However, since a full implicit resolution of the particle positions and of the fields is virtually impossible, a two-step predictor-corrector approximation is practically implemented. In the implicit moment method, a prediction of the value of the fields at the next time step is done through the use of the moment equations. Numerous extensions of these methods can be found in the literature, especially concerning the coupling with the Maxwell equations [4, 25, 32, 35, 36, 41].
Recently, new classes of methods for singular perturbation problems have emerged. These are the so-called Asymptotic-Preserving (AP) methods. Let (S_λ) be a singularly perturbed system and (S_0) the limit system when $\lambda \to 0$. In our case, (S_λ) is the Vlasov-Poisson system and (S_0) is the quasineutral Vlasov system. An Asymptotic Preserving scheme for (S_λ) in the limit $\lambda \to 0$ is a scheme which is consistent with (S_λ) when the numerical parameters (e.g. Δx, Δt) resolve the scales associated with the small parameter λ and which is consistent with (S_0) when $\lambda \to 0$ with Δt, Δx staying of order one. The concept of AP method originates from the work of Shi Jin for multiscale kinetic equations [28].
The concept of AP method is particularly interesting when λ is not uniformly small. For instance, at a plasma edge, the parameter λ, which depends on the local value of the plasma density, can vary by several orders of magnitude

from $\lambda \ll 1$ to $\lambda = O(1)$. In this case, the original problem (S_λ) must be solved in the region where $\lambda = O(1)$ and the limit problem (S_0), where $\lambda \ll 1$. With classical method, this situation requires a model coupling methodology to connect the two models. However, model coupling methods involve a certain level of arbitrariness, such as the location of the coupling interface or the expression of the coupling terms. Their implementation can also be quite complex with the need to adapt the mesh to the geometry of the interface. The AP method allows the computation of the two regions $\lambda = O(1)$ and $\lambda \ll 1$ with the same and unique method. The AP scheme automatically shifts from the (S_λ) model to the (S_0) model wherever λ becomes small, without any need to reduce the time and space steps. This results in a considerably more robust numerical code. We shall see an example of this situation with the simulation of the expansion of an ion slab at section 4.2.
In this paper, we propose an Asymptotic Preserving PIC method (or PICAP method) for the Vlasov-Poisson equation in the quasineutral limit. Previous works on AP methods for the quasineutral limit have been devoted to the Euler-Poisson problem [10, 12, 14] and to Eulerian schemes for the Vlasov-Poisson problem [2]. The quasineutral limit in plasmas has been theoretically investigated in [5, 11, 20, 21, 24, 37].
The present work is a follow-up of a previous work [13], where a first variant of the method (the PICAP-1 method) was presented and tested on a one-species model of a perturbed Maxwellian plasma. In the present work, we introduce a new, simpler variant of this method (the PICAP-2 method) and test it for both one and two-species situations. The use of the realistic electron to ion mass ratio makes the two-species case a much stiffer test problem. We will also consider a problem consisting of the expansion of an ion slab as a benchmark problem. This problem has been proposed by [22, 23], where both analytical and numerical solutions can be found.
The method relies on the remark that the equation allowing the computation of the potential in the quasineutral Vlasov problem is very different from the Poisson equation. Indeed, the former is an elliptic equation found from the divergence free condition on the current, a consequence of the quasineutrality. To build an AP scheme, it is necessary to find a unified framework for both the Poisson equation and the quasineutral potential equation. This is done by reformulating the Poisson equation into a strictly equivalent equation which explicitly contains the quasineutral potential equation as a particular case when $\lambda = 0$. This equation is differential in both time and space, and specifically second order in time. An implicit discretization of this equation

is combined with a semi-implicit discretization of the particle trajectories and yields an Asymptotic-Preserving scheme for the Vlasov-Poisson problem in the quasineutral limit. Since the reformulation of the Poisson equation leads to a fully equivalent problem, there is no other approximation involved in our method than purely numerical ones (i.e. associated to the time and space discretization). To our knowledge, previous implicit methods such as the direct implicit or the moment implicit ones (see references above) have not been analyzed in view of this Asymptotic Preservation property, and it is not known whether they satisfy it or not.
This paper is organized as follows. In section 2, we present the two-fluid Vlasov-Poisson system model and its quasineutral limit and we derive the reformulated Poisson equation. ¿From this reformulation, in section 3, we build up the Asymptotic-Preserving Particle-In-Cell (PICAP) method. Section 4 is devoted to the discussion of the numerical results: comparisons between the classical and asymptotic preserving schemes are provided in a one-dimensional geometry. We consider two test problems consisting firstly of a periodic perturbation of Maxwellian plasma and secondly of a plasma expansion in the vacuum as investigated in [22, 23]. The results confirm that the AP strategy remains stable and provides the expected results even if the time and space discretizations do not resolve the Debye length and plasma periods. This shows that the method can powerfully deal with stiff problems when the stiffness results from the quasineutrality constraint.

2 The Vlasov-Poisson system and its quasineutral limit

In this section, we present the two-fluid Vlasov-Poisson system and its quasineutral limit.

2.1 The Vlasov-Poisson system

We are interested in the kinetic description of a two-fluid plasma constituted of electrons and one ion species. Then, ions and electrons are described by their distribution function respectively denoted by $f_i(x, v, t)$ and $f_e(x, v, t)$, where the position and velocity variables x and v are such that $(x, v) \in \Omega \times \mathbb{R}^d$, with $\Omega \subset \mathbb{R}^d$ and $d = 1$, 2, or 3 and $t \geq 0$ is the time. The two-fluid Vlasov-Poisson system is written:

$$\partial_t f_i + v \cdot \nabla_x f_i - \frac{e}{m_i} \nabla_x \phi \cdot \nabla_v f_i = 0, \tag{2.1}$$

$$\partial_t f_e + v \cdot \nabla_x f_e + \frac{e}{m_e} \nabla_x \phi \cdot \nabla_v f_e = 0, \tag{2.2}$$

where we denote by $e > 0$ the positive elementary charge, by $m_{i,e}$ the ion and electron masses and by ϕ the electric potential. ϕ is given by the Poisson equation:

$$-\Delta \phi = \frac{e}{\varepsilon_0}(n_i - n_e), \tag{2.3}$$

where ε_0 is the vacuum permittivity, and $n_{i,e}$ are the ion and electron densities, given by

$$n_i(x,t) = \int_{\mathbb{R}^d} f_i(x,v,t)dv, \qquad n_e(x,t) = \int_{\mathbb{R}^d} f_e(x,v,t)dv.$$

The two important physical scales for this model are the Debye length λ_D and the electron plasma frequency ω_p given by:

$$\lambda_D = \Big(\frac{\varepsilon_0 k_B T_0}{e^2 n_0}\Big)^{1/2}, \qquad \omega_p = \Big(\frac{n_0 e^2}{\varepsilon_0 m_e}\Big)^{1/2},$$

where k_B is the Boltzmann constant, n_0 is the plasma density scale ($n_0 \backsim n_i \backsim n_e$), T_0 is the plasma temperature scale. We note that an ion plasma frequency can be defined (replacing m_e by m_i). However, this parameter is smaller than ω_p because of the large ion to electron mass ratio. The electron plasma period is defined by $\tau_p = 1/\omega_p$.

The situation where both the Debye length and electron plasma period are very small compared with the typical macroscopic length and time scales is called the quasineutral regime because the local electric charge vanishes everywhere. However, since the electron plasma period becomes simultaneously very small, local charge unbalances (at the scale of the Debye length) induce very high plasma frequency oscillations.

In order to study the quasineutral model, we introduce the following scaling of the Vlasov-Poisson problem. The scaled variables are given by

$$\bar{x} = \frac{x}{x_0},\ \bar{v} = \frac{v}{v_0},\ \bar{t} = \frac{v_0}{x_0}t,\ \bar{n}_{i,e} = \frac{n_{i,e}}{n_0},\ \bar{f}_{i,e} = \frac{v_0}{n_0} f_{i,e}, \bar{\phi} = \frac{e\phi}{k_B T_0}, \tag{2.4}$$

where $x_0 > 0$ is the typical length of the problem, and $v_0 \in \mathbb{R}$ is the thermal ion velocity scale given by $v_0 = (k_B T_0/m_i)^{1/2}$. Inserting this scaling into equations (2.1)-(2.3) and omitting the bars, we get the following scaled two-fluid Vlasov-Poisson model

$$\partial_t f_i + v \cdot \nabla_x f_i - \nabla_x \phi \cdot \nabla_v f_i = 0, \tag{2.5}$$

$$\partial_t f_e + v \cdot \nabla_x f_e + \frac{1}{\varepsilon} \nabla_x \phi \cdot \nabla_v f_e = 0, \tag{2.6}$$

$$-\lambda^2 \Delta \phi = (n_i - n_e), \quad n_{i,e} = \int f_{i,e}\, dv. \tag{2.7}$$

where $\lambda = \lambda_D/L$ is the scaled Debye length and $\varepsilon = m_e/m_i$ is the electron to ion mass ratio. Note that the scaled plasma frequency is given by $\omega = \omega_p x_0/v_0 = 1/(\sqrt{\varepsilon}\lambda)$. In the following, we investigate the limit $\lambda \to 0$ which leads to the quasineutral limit.

In the forthcoming test cases, we will also be interested in the one-species case, considering only electrons while ions are supposed static (due to their very large mass). The scaled one-species Vlasov-Poisson problem is written:

$$\partial_t f + v \cdot \nabla_x f + \nabla_x \phi \cdot \nabla_v f = 0, \tag{2.8}$$

$$-\lambda^2 \Delta \phi = (n_0 - n), \quad n = \int f\, dv\,, \tag{2.9}$$

where n_0 is supposed to be a uniform ion background density.

2.2 Reformulation of the Poisson equation

The quasineutral limit consists in letting $\lambda \to 0$ in the scaled Vlasov-Poisson system (2.5)-(2.7). Obviously, when $\lambda = 0$, we lose the possibility of using the Poisson equation (2.7) to compute the potential ϕ since (2.7) reduces to the quasineutrality constraint $n_i = n_e$. For this reason, we introduce a reformulation of the problem which provides a more convenient approach to the quasineutral limit.

To this aim, we take the velocity moments of eqs. (2.5) and (2.6) and obtain the mass and momentum conservation equations:

$$\partial_t n_i + \nabla \cdot (nu)_i = 0, \tag{2.10}$$

$$\partial_t (nu)_i + \nabla \cdot S_i = -n_i \nabla \phi, \tag{2.11}$$

$$\partial_t n_e + \nabla \cdot (nu)_e = 0, \tag{2.12}$$

$$\partial_t (nu)_e + \nabla \cdot S_e = \frac{n_e}{\varepsilon} \nabla \phi, \tag{2.13}$$

where $(nu)_{i,e}$, the ion and electron momenta and $S_{i,e}$, the (specific) momentum fluxes are given by

$$(nu)_{i,e} = \int_{\mathbb{R}^d} f_{i,e}(x,v,t)\, v\, dv, \qquad S_{i,e} = \int_{\mathbb{R}^d} f_{i,e}(x,v,t)\, v \otimes v\, dv,$$

and the symbol $\otimes$ denotes the tensor product. Taking the differences of (2.10) and (2.12) on the one hand, and of (2.11) and (2.13) on the other hand, we get the continuity and current equations respectively:

$$\partial_t(n_i - n_e) + \nabla \cdot ((nu)_i - (nu)_e) = 0. \tag{2.14}$$

$$\partial_t((nu)_i - (nu)_e) + \nabla \cdot (S_i - S_e) = -(n_i + \frac{n_e}{\varepsilon})\nabla\phi. \tag{2.15}$$

Taking the time derivative again of (2.14) and the divergence of (2.15) and subtracting the resulting two equations leads to:

$$\partial_t^2(n_i - n_e) - \nabla^2 : (S_i - S_e) = \nabla \cdot \Big(\Big(n_i + \frac{n_e}{\varepsilon}\Big)\nabla\phi\Big), \tag{2.16}$$

where ∇^2 denotes the tensor of second order derivatives and ":" the contracted product of two tensors. After substitution of the Poisson equation (2.7), this equation yields:

$$-\lambda^2\partial_t^2\Delta\phi - \nabla^2 : (S_i - S_e) = \nabla \cdot \Big(\Big(n_i + \frac{n_e}{\varepsilon}\Big)\nabla\phi\Big). \tag{2.17}$$

Collecting ϕ into the left-hand side, we find the so-called reformulated Poisson equation:

$$-\nabla \cdot \Big(\Big(n_i + \frac{n_e}{\varepsilon} + \lambda^2\partial_t^2\Big)\nabla\phi\Big) = \nabla^2 : (S_i - S_e). \tag{2.18}$$

These computations show that, if the triple (f_e, f_i, ϕ) solves the Vlasov-Poisson problem (2.5)-(2.7), it solves the "reformulated Vlasov-Poisson problem" consisting of the Vlasov equations (2.5), (2.6) and the reformulated Poisson equation (2.18). Conversely, if the triple (f_e, f_i, ϕ) solves the reformulated Vlasov-Poisson problem, we find, going backwards in the previous computations, that ϕ satisfies:

$$\partial_t^2(-\lambda^2\Delta\phi - (n_i - n_e)) = 0.$$

Therefore, if the initial data $\phi_0 := \phi|_{t=0}$ and $\phi_0' := (\partial_t\phi)|_{t=0}$ satisfy the two Poisson equations at the initial time:

$$-\lambda^2\Delta\phi_0 = (n_i - n_e)_0, \tag{2.19}$$

$$-\lambda^2\Delta\phi_0' = (n_i - n_e)_0' = -\nabla \cdot ((nu)_i - (nu)_e)_0, \tag{2.20}$$

(with obvious notations), then the Poisson equation (2.7) is satisfied at all times. Since eq. (2.18) is second order in time, it requires the knowledge of the two initial conditions ϕ_0 and ϕ_0'. Therefore, it is always possible to impose (2.19) and (2.20).
We can summarize this discussion by saying that the Vlasov-Poisson system (2.5)-(2.7) is **equivalent** to the following **"reformulated Vlasov-Poisson system"**:

$$\partial_t f_i + v \cdot \nabla_x f_i - \nabla_x \phi \cdot \nabla_v f_i = 0, \tag{2.21}$$

$$\partial_t f_e + v \cdot \nabla_x f_e + \frac{1}{\varepsilon} \nabla_x \phi \cdot \nabla_v f_e = 0, \tag{2.22}$$

$$-\nabla \cdot \Big(\Big(n_i + \frac{n_e}{\varepsilon} + \lambda^2 \partial_t^2 \Big) \nabla \phi \Big) = \nabla^2 : (S_i - S_e), \tag{2.23}$$

with ϕ satisfying the initial conditions (2.19), (2.20).
The reformulated Poisson equation has been previously proposed in the framework of fluid models in [10, 12, 14], and in [2, 13] for plasma kinetic models.

2.3 The quasineutral limit

The quasineutral limit of the Vlasov-Poisson system has been investigated theoretically in [5, 20, 21] and extensively used in physical studies. It is almost impossible to cite all the relevant physical literature. We just mention [26, 29, 39] as examples.
The reformulation (2.21)-(2.23) allows to investigate the quasineutral limit $\lambda \to 0$ in a straightforward way. Indeed, letting $\lambda \to 0$ in (2.23), (2.19), (2.20) directly provides the following equation for the quasineutral potential ϕ:

$$-\nabla \cdot \Big(\Big(n_i + \frac{n_e}{\varepsilon} \Big) \nabla \phi \Big) = \nabla^2 : (S_i - S_e), \tag{2.24}$$

together with the two constraints

$$(n_i - n_e)_0 = 0, \tag{2.25}$$

$$(n_i - n_e)_0' = -\nabla \cdot ((nu)_i - (nu)_e)_0 = 0, \tag{2.26}$$

¿From these equations and with the aid of (2.16), we immediately deduce that $n_i = n_e$ at all times, which shows that quasineutrality holds.

Therefore, the limit $\lambda \to 0$ of the Vlasov-Poisson system (2.5)-(2.7), or equivalently, of its reformulation (2.21)-(2.23) leads to the following **quasineutral Vlasov system**:

$$\partial_t f_i + v \cdot \nabla_x f_i - \nabla_x \phi \cdot \nabla_v f_i = 0, \tag{2.27}$$

$$\partial_t f_e + v \cdot \nabla_x f_e + \frac{1}{\varepsilon} \nabla_x \phi \cdot \nabla_v f_e = 0, \tag{2.28}$$

$$-\nabla \cdot \left(\left(n_i + \frac{n_e}{\varepsilon} \right) \nabla \phi \right) = \nabla^2 : (S_i - S_e), \tag{2.29}$$

together with the initial conditions satisfying (2.25), (2.26).
We see that, although the original and reformulated Vlasov-Poisson systems are equivalent, they are not equally well-suited in the quasineutral limit. Indeed, the quasineutral potential eq. (2.29) appears as the formal limit $\lambda \to 0$ of the reformulated Poisson eq. (2.23) but not of the original Poisson eq. (2.7). The asymptotics does not preserve the form of the original Poisson equation while it does preserve the form of the reformulated one. Therefore, the construction of Asymptotic-Preserving schemes must be based on the use of the reformulated Poisson equation. For this reason, our Asymptotic-Preserving PIC method relies on the numerical approximation of the reformulated Vlasov-Poisson problem (2.21)-(2.23) rather than that of the original Vlasov-Poisson problem (2.5)-(2.7). We now describe the method in detail in the next section.

3 Asymptotic-Preserving PIC method (PICAP method)

3.1 PIC methods: general methodology

Particle-in-Cell (PIC) methods are widely used in the plasma physics community. We refer to the text books [3, 27] for a detailed exposition (see also the bibliography in section 1). The particle method consists in discretizing $f_{i,e}$ into a sum of delta measures located at positions $((X_{i,e})_j(t), (V_{i,e})_j(t))$ in phase space. This is written:

$$\begin{aligned} f_{i,e}(x,v,t) &\approx (f_{i,e})_N(x,v,t) \\ &:= \sum_{j=1}^{N} (\omega_{i,e})_j \, \delta\left(x - (X_{i,e})_j(t)\right) \, \delta\left(v - (V_{i,e})_j(t)\right) , \end{aligned} \tag{3.1}$$

where N is the number of particles and $(\omega_{i,e})_j$ is a weight which must be conveniently defined at initialization [3, 27]. The j-th particle coordinates $((X_{i,e})_j(t), (V_{i,e})_j(t))$ obey Newton's equations:

$$(\dot{X}_i)_j = (V_i)_j\,, \quad (\dot{V}_i)_j = -\nabla_x \phi_h((X_i)_j(t), t)\,, \tag{3.2}$$

$$(\dot{X}_e)_j = (V_e)_j\,, \quad (\dot{V}_e)_j = \frac{1}{\varepsilon}\nabla_x \phi_h((X_e)_j(t), t)\,, \tag{3.3}$$

These equations are discretized in time (see discussion below). The potential ϕ_h is a space approximation of ϕ. In the PIC method, this approximation is computed at each time step by solving the Poisson eq. (2.7) on a fixed grid of space step h (e.g. using a finite difference method). An assignment procedure allows to build grid values of the particle densities $(n_{i,e})_h$ from the knowledge of the particle locations and weights. These values serve as data for the numerical resolution of the Poisson equation. Once an approximation ϕ_h on the grid has been obtained, an interpolation procedure allows to reconstruct the values of the field $\nabla_x \phi_h(X_j, t)$ at the locations of the particles. These assignment-interpolation procedures are classical and are not modified in the present work (see again [3, 27]). The only modification resulting from the replacement of the original Poisson equation (2.7) by the reformulated one (2.23) is the need to assign other quantities than the densities, namely the values of the pressure tensors $S_{i,e}$. However, the assignment procedure for these quantities is the same as for the densities and does not require a specific discussion.

The major issue in making the PIC procedure Asymptotic-Preserving, besides using the reformulated Poisson equation instead of the original one, is the time discretization. The classical time-stepping method is a "leap-frog" scheme where positions are defined at integer values of the time step $X_j^m \approx X_j(m\Delta t)$, while velocities are defined at half-integer values $V_j^{m+1/2} \approx V_j((m+1/2)\Delta t)$. In classical PIC method, the integration of (3.2), (3.3) is done as follows:

$$\frac{(X_{i,e})_j^{m+1} - (X_{i,e})_j^m}{\Delta t} = (V_{i,e})_j^{m+1/2}, \tag{3.4}$$

$$\frac{(V_i)_j^{m+3/2} - (V_i)_j^{m+1/2}}{\Delta t} = -\nabla_x \phi^{m+1}((X_i)_j^{m+1}), \tag{3.5}$$

$$\frac{(V_e)_j^{m+3/2} - (V_e)_j^{m+1/2}}{\Delta t} = \frac{1}{\varepsilon}\nabla_x \phi^{m+1}((X_e)_j^{m+1}), \tag{3.6}$$

where we omit the index h for the grid-approximation of the potential for simplicity. Advancing the velocities with (3.5), (3.6) supposes that Poisson's equation is solved with positions at time t^{m+1}, which is possible since these are known from (3.4). However, it is well known and widely documented in the literature [3, 27] that this method suffers from a stability constraint of the form $\Delta t, h \leq C\lambda$ where the constant C is of order of unity. We shall refer to this scheme as the standard PIC scheme. There have been numerous attempts to provide more stable time-stepping strategies (see the bibliography in section 1) which have proved to be quite efficient in practical cases. However, it is not clear if these methods are consistent with the quasineutral Vlasov model (2.27)-(2.29) in the limit $\lambda \to 0$. The PICAP methods which we are going to discuss now do have this property, as we will show below.

3.2 PICAP method: time advancement scheme

In the proposed Asymptotic Preserving strategy, positions and velocities are both defined at integer time-steps for simplicity. The time-stepping method for the position equation is fully implicit while that of the velocity equation is semi-implicit: the electric field is taken implicitly but the particle positions explicitly. More precisely, the particle time advancement scheme is as follows:

$$\frac{(X_{i,e})_j^{m+1} - (X_{i,e})_j^m}{\Delta t} = (V_{i,e})_j^{m+1}, \tag{3.7}$$

$$\frac{(V_i)_j^{m+1} - (V_i)_j^m}{\Delta t} = -\nabla_x \phi^{m+1}((X_i)_j^m), \tag{3.8}$$

$$\frac{(V_e)_j^{m+1} - (V_e)_j^m}{\Delta t} = \frac{1}{\varepsilon}\nabla_x \phi^{m+1}((X_e)_j^m). \tag{3.9}$$

The implicit evaluation of the potential ϕ^{m+1} is obtained via an implicit time-discretization of the reformulated Poisson equation (2.23).
The starting point for our implicit time-discretization of (2.23) is the following scheme:

$$-\nabla_x \cdot \Big((\Delta t)^2(n_i^m + \frac{n_e^m}{\varepsilon})\nabla_x \phi^{m+1} + \lambda^2(\nabla_x \phi^{m+1} - 2\nabla_x \phi^m + \nabla_x \phi^{m-1})\Big) = \\ = (\Delta t)^2 \nabla_x^2 : (S_i^m - S_e^m). \tag{3.10}$$

This scheme is clearly Asymptotic-Preserving. Indeed, in the limit $\lambda \to 0$, we find

$$-\nabla_x \cdot \left((n_i^m + \frac{n_e^m}{\varepsilon}) \nabla_x \phi^{m+1} \right) = \nabla_x^2 : (S_i^m - S_e^m). \tag{3.11}$$

which is a consistent discretization of the quasineutral potential eq. (2.29). However, the presence of the Laplacians of the potential at the previous time steps ϕ^m and ϕ^{m-1} at the left-hand side of (3.10) is somehow inconvenient. It introduces an extra computational cost and additionally, can lead to large truncation errors if ϕ suffers from fluctuations. Therefore, it is more natural to use the Poisson eq. (2.7) to replace these terms by the charge densities at the corresponding time steps.
To this aim, two strategies have been proposed. The first method, already proposed in [13] and called "PICAP-1", consists in simply performing this replacement. It leads to:

$$\begin{aligned} -\nabla \cdot \left(((\Delta t)^2 (n_i^m + \frac{n_e^m}{\varepsilon}) + \lambda^2) \nabla \phi^{m+1} \right) \\ = (\Delta t)^2 \nabla^2 : (S_i^m - S_e^m) + 2(n_i^m - n_e^m) - (n_i^{m-1} - n_e^{m-1}). \end{aligned} \tag{3.12}$$

Eq. (3.12) allows to compute ϕ^{m+1} from known quantities at time t^m and t^{m-1}.
Another, original method is found by using a time-discrete version of the continuity eq. (2.14) to replace the term $(n_i^m - n_e^m) - (n_i^{m-1} - n_e^{m-1})$ at the right-hand side of (3.12) by $-\nabla((nu)_i^m - (nu)_e^m)$. This leads to the so-called "PICAP-2" method:

$$\begin{aligned} -\nabla \cdot \left(((\Delta t)^2 (n_i^m + \frac{n_e^m}{\varepsilon}) + \lambda^2) \nabla \phi^{m+1} \right) \\ = (\Delta t)^2 \nabla^2 : (S_i^m - S_e^m) + (n_i^m - n_e^m) - \Delta t (\nabla((nu)_i^m - (nu)_e^m)), \end{aligned} \tag{3.13}$$

which allows to compute ϕ^{m+1} from known quantities at time t^m alone.
The advantage of the PICAP-2 method is that it does not require an auxiliary scheme to compute the first iterate at time t^1, while PICAP-1 does. The computation of the first iterate requires the use of the standard PIC scheme. But if λ is very small, the use of the classical PIC scheme over a single time step can be enough to trigger an instability of the whole method. Therefore, the use of the PICAP-2 method is preferable.
In spite of the presence of the extra terms at the right-hand sides of (3.12) and (3.13) the PICAP-1 and PICAP-2 methods are Asymptotic-Preserving.

Indeed, at each time step, both differ from the AP method (3.10) by terms which are proportional to $n_i - n_e$ and which consequently are of order $O(\lambda^2)$. Therefore, these additional terms vanish in the limit $\lambda \to 0$ and the PICAP-1 and PICAP-2 methods are Asymptotic-Preserving as well. The numerical experiments below provide an experimental evidence of this statement.

3.3 Full discretization of the reformulated Poisson equation

In this section, for the sake of completeness, we describe the space discretization of the time semi-discretized equations (3.12) and (3.13). Here, we restrict to the one-dimensional case but the multidimensional extension of the method on a cartesian uniform grid is straightforward.
Let Δx be a uniform space step and $x_k = k\Delta x$, $k \in \mathbb{Z}$. Let $g_k \approx g(x_k)$ be the sequence of approximate values of the function g on the space grid. We set

$$
\begin{aligned}
(D^+ g)_k &= \frac{g_{k+1} - g_k}{\Delta x}, \\
(D^- g)_k &= \frac{g_k - g_{k-1}}{\Delta x}, \\
(\Delta_{ap} g)_k &= (D^+ D^- g)_k = (D^- D^+ g)_k = \frac{g_{k+1} - 2g_k + g_{k-1}}{(\Delta x)^2}.
\end{aligned}
$$

The space discretization of the PICAP-1 reformulated Poisson equation is given by:

$$
\begin{aligned}
-\frac{\lambda^2}{(\Delta t)^2}(\Delta_{ap}\phi)_k^{m+1} - \left(D^- \big(((n_i)^m + \frac{(n_e)^m}{\varepsilon}) D^+ \phi^{m+1} \big) \right)_k = \\
(\Delta_{ap}((S_i)^m - (S_e)^m))_k + \frac{2((n_i)_k^m - (n_e)_k^m) - ((n_i)_k^{m-1} - (n_e)_k^{m-1})}{(\Delta t)^2}.
\end{aligned}
\tag{3.14}
$$

This equation involves the inversion of the following matrix, which is the

approximation of the elliptic operator at the left-hand side of (3.12):

$$
\begin{aligned}
(A^m\phi)_k &= -\frac{\lambda^2}{(\Delta t)^2}(\Delta_{ap}\phi)_k - \left(D^-\big(((n_i)^m + \frac{(n_e)^m}{\varepsilon})D^+\phi\big)\right)_k \\
&= \left(\frac{2\lambda^2}{(\Delta t)^2(\Delta x)^2} + \frac{(n_i^m + \frac{n_e^m}{\varepsilon})_k}{(\Delta x)^2} + \frac{(n_i^m + \frac{n_e^m}{\varepsilon})_{k-1}}{(\Delta x)^2} \right)\phi_k \\
&\quad - \left(\frac{\lambda^2}{(\Delta t)^2(\Delta x)^2} + \frac{(n_i^m + \frac{n_e^m}{\varepsilon})_k}{(\Delta x)^2} \right)\phi_{k+1} \\
&\quad - \left(\frac{\lambda^2}{(\Delta t)^2(\Delta x)^2} + \frac{(n_i^m + \frac{n_e^m}{\varepsilon})_{k-1}}{(\Delta x)^2} \right)\phi_{k-1}.
\end{aligned}
$$

The space discretization of the PICAP-2 reformulated Poisson equation is given by:

$$
\begin{aligned}
-\frac{\lambda^2}{(\Delta t)^2}(\Delta_{ap}\phi)_k^{m+1} &- \left(D^-\big(((n_i)^m + \frac{(n_e)^m}{\varepsilon})D^+\phi^{m+1}\big)\right)_k \\
&= (\Delta_{ap}((S_i)^m - (S_e)^m))_k - \frac{(D^-((n_iu_i)^m - (n_eu_e)^m))_k)}{\Delta t} \\
&\quad + \frac{((n_i)_k^m - (n_e)_k^m)}{(\Delta t)^2}. \qquad (3.15)
\end{aligned}
$$

It involves the inversion of the same matrix A^m. Only the right-hand side is different.

4 Numerical results

In this section we show numerical results in one space dimension for the Vlasov-Poisson system. We simulate two test-cases and we compare the results obtained with the Classical PIC, PICAP-1 and PICAP-2 schemes. The first test-case consists in a perturbation of a Maxwellian plasma and the second test-case is a plasma expansion in vacuum.

4.1 Periodic perturbation of a quasineutral Maxwellian plasma

In this section, we propose to validate the method using the same test problem as in the short note [13] i.e. a small perturbation of a Maxwellian plasma.

We perform the simulation on the domain $(0, 1)$ with periodic boundary conditions for the Vlasov system and with homogeneous Dirichlet boundary conditions for the Poisson equation.
We consider successively the one-species case (i.e. system (2.8)-(2.9)) and the two-species case (i.e. system (2.5)-(2.7)). In [13], only the one-species case was considered. In the two-species case, we choose a realistic mass ratio $\varepsilon = 10^{-4}$. The PICAP schemes seem robust even in the case of realistic electron to ion mass ratios. However, ideally, an Asymptotic-Preserving scheme for both the limits $\lambda \to 0$ and $\varepsilon \to 0$ should be sought. This problem is still under current investigation.

4.1.1 Periodic perturbation: one species case

For this case, we develop the PICAP-1 and PICAP-2 schemes for system (2.8)-(2.9). We select $\lambda = 10^{-4}$ which means that the scaled plasma frequency has the value $\omega = \frac{1}{\lambda} = 10^4$ and we use 100 particles per cell. We initialize the Vlasov-Poisson equation with

$$f_0 = \pi^{-1/2}(1 + \delta \sin(\kappa\pi x)) \exp(-v^2), \qquad n_0 = 1. \tag{4.1}$$

where $\delta = 10^{-2}$ is the perturbation amplitude and $\kappa = 2220$. This test-case has been already considered in the short note [13]. The value of κ is chosen such that $\kappa \sim \lambda^{-1}$ to ensure that the wavelength of the density perturbation is of the same order as the Debye length. In this case, the phase velocity of the wave (which is nearly ω_p/κ in physical units) is of the same order as the thermal velocity v_{th} (which in our dimensionless units, is unity). This situation corresponds to a strong particle-wave coupling [7, 30], since the thermal velocity roughly coincides with the location of the steepest slope of the velocity distribution function.
We note that in many references, particularly dealing with Eulerian solvers such as [16], the value of κ is chosen of order one. The reason is that the target of such methods is the accurate resolution of such phenomena as nonlinear Landau damping, plasma echoes, etc. The target of the PICAP method is different. The method is aimed at simulations on times scales which are large compared with the plasma period. The method is not expected to be accurate enough for a fine analysis of phenomena occurring at scales comparable with the plasma period and is actually not designed for that. This is the reason why we discard such tests.

In Fig. 1, we present results obtained with the classical PIC, PICAP-1 and PICAP-2 schemes when $\Delta x = \lambda = 10^{-4}$. The time step Δt satisfies both CFL conditions $v_{\max}\Delta t \leq \Delta x$ and $\omega\Delta t \leq 1$, where $v_{\max}$ is the maximal electron velocity at each time step. In these conditions, the fast space and time scales (respectively the Debye length and plasma period) are both resolved. Fig. 1 (left) gives the electric potential as a function of position at an instant $t = 10\,\omega^{-1} = 10^{-3}$. The electric potential is almost identical with the three schemes. The electric potential as a function of position is shown on Fig. 1 (right) after a large number of plasma periods ($t = 2000\,\omega^{-1} = 0.2$). We can see that the amplitude of the plasma waves is of the same order of magnitude as previously when using the classical PIC scheme, while it has been strongly damped out with the PICAP-1 and PICAP-2 methods. This shows that the AP strategy damps out the energy of the plasma waves and allows to capture phenomena which occur on longer time scales.

Fig. 2 now shows the results obtained when the fast space and time scales are both under-resolved, i.e. the space step is larger than the Debye length $\Delta x > \lambda$ and the time step is larger that the plasma period $\Delta t > \omega^{-1}$. We choose $\Delta x = 10^{-2}$ while $\lambda = 10^{-4}$ is unchanged. Meanwhile, the total number of particles is kept unchanged. For both PICAP-1 and PICAP-2 schemes, we use a time step determined by the CFL conditions: $v_{\max}\Delta t \leq \Delta x$. In Fig. 4, we plot $\omega\Delta t$ as a function of time. We see that this constraint still allows Δt of the order of 30 times the plasma period ω^{-1}. Simultaneously, we use a uniform time step for the Classical PIC scheme, with $\Delta t = 30\omega^{-1}$. We cannot use the CFL condition because the instability generates very large particle velocities and enforcing the CFL condition would generate very small time steps.

Fig. 2 depicts the electric potential as a function of space, at time $t = 0.2$. The left picture show the result using the classical PIC scheme. The instability of the scheme is clearly visible since the amplitude of the potential oscillations are now of the order of ten times those of the initial potential (see Fig. 1 for instance). With the PICAP-1 or PICAP-2 schemes, these amplitudes are now very small showing that the schemes are stable and have damped out plasma waves, as in the resolved case.

Fig. 3 displays the total energy $\mathcal{E}$ (in log scale) as a function of time for the different schemes in the resolved and under-resolved situations. For the exact solution of the Vlasov-Poisson equation (one-species case), the total energy

$\mathcal{E}$ is given by

$$\mathcal{E} = \frac{\lambda^2}{2} \int |\partial_x \phi|^2 dx + \frac{1}{2} \int f|v|^2 dx dv, \tag{4.2}$$

and is constant in time. Fig. 3 (left) shows the resolved case. We notice that the total energy for the classical PIC scheme decays slowly after a more rapid initial transient. By contrast, the total energy of both PICAP-1 and PICAP-2 schemes decays more steadily. In Fig. 3 (right), the under-resolved case is considered. With the Classical PIC scheme, the total energy is unstable and reaches large and totally unrealistic values after a very rapid initial transient. With the AP schemes, they are both stable and damped to zero. We note that the PICAP-2 scheme seems to exhibit a slower energy decay than the PICAP-1 scheme which has been initially proposed in [13]. Paradoxically, the energy decay of the PICAP-1 and PICAP-2 seems far less pronounced in the under-resolved case than in the resolved case.

In [13], the energy damping has been attributed to the noisy coefficients of the reformulated Poisson equations (3.14) (because the densities and the tensors S have to be computed from the particles and because additionally, a second order space derivative of S is needed as a source term in this equation). It has been noticed that, if high frequencies are cut off in order to eliminate the noise, the energy damping can be significantly reduced. The application of filtering techniques, or more generally, of noise reduction techniques to these new PICAP schemes will be the subject of future studies.

When the fast space scale is under-resolved but the fast time scale is resolved, the Classical PIC scheme is still unstable. We have performed simulations with $\Delta x = 10^{-2}$, $\lambda = 10^{-4}$ and $\Delta t = 0.9\omega^{-1}$. The results are very similar to those obtained in the fully (time and space) under-resolved case (and for this reason, the results are not displayed). This is to be compared to the behaviour of classical schemes for the fluid models (i.e. the Euler-Poisson problem in the quasineutral limit) [12], where it has been observed that the results are stable as long as the fast time scale is resolved, even if the fast space scale is under-resolved. It looks as if the kinetic problem was more unstable than the fluid one, since as soon as one of the fast time or space scale is under-resolved, the scheme becomes unstable. By contrast, both the PICAP-1 and PICAP-2 schemes are stable. The results are very similar to those of the fully resolved case and are not represented.

4.1.2 Periodic perturbation: two species case

In this section, we consider the two species problem (2.5)-(2.7) and choose the following parameters:

$$\varepsilon = 10^{-4}, \qquad \lambda = 10^{-4} \qquad \Big(\omega = \frac{1}{\lambda\sqrt{\varepsilon}} = 10^{6}\Big).$$

Again, we put 100 ions and 100 electrons in each cell. We initialize this test-case with

$$\begin{aligned} f_{e0} &= \varepsilon\,\pi^{-1/2}(1+\delta\sin(\kappa\pi x))\exp(-\varepsilon v^2), \\ f_{i0} &= \pi^{-1/2}(1+\delta\sin(\kappa\pi x))\exp(-v^2). \end{aligned}$$

with $\delta = 10^{-2}$ and $\kappa = 2220$.
We first consider the case where the Debye length and electron plasma period are both resolved ($\Delta x = \lambda$, $\Delta t < \omega^{-1}$). In Fig. 5 (left), we plot the electric potential after three plasma periods $t = 3\omega^{-1} = 3\times 10^{-6}$. We can see that the Classical PIC scheme and PICAP schemes are almost identical. After 8000 plasma periods (i.e. scaled time $t = 8\times 10^{-3}$), Fig. 5 (right) shows that the electric potential has been more strongly dissipated with the PICAP schemes than with the classical PIC schemes. The amount of dissipation is stronger than in the one-species case.
When none of the Debye length and plasma period are resolved, the same quantities are plotted in Fig. 6. The time-step is chosen to satisfy the CFL condition: $\Delta t = 0.9\Delta x/v_{\max}$. Fig. 8 shows the evolution of the time step as a function of time. We notice that the time step reaches values which are of the order of 25 times the plasma period. For the standard PIC scheme, the time step is kept fixed at this value for the same reason as explained above. We observe that the electric potential obtained with the classical PIC scheme develops an instability while those obtained with the PICAP schemes remain stable.
In the two-species case, the total energy of the Vlasov-Poisson problem is given by

$$\mathcal{E} = \frac{\lambda^2}{2}\int |\partial_x\phi|^2 dx + \frac{1}{2}\int f_i|v|^2 dxdv + \frac{\varepsilon}{2}\int f_e|v|^2 dxdv, \tag{4.3}$$

and is constant in time. The total energy (in log scales) as a function of time is displayed in Fig. 7, in the resolved case (left) and under-resolved

one (right). The conclusions are the same as in the one-species case: the energy dissipation of the Classical PIC scheme is lower than that of the two AP schemes in the resolved case. However, in the under-resolved case, the Classical PIC scheme exhibits a severe instability while the two AP schemes are still stable. Additionally, the energy dissipations of the AP schemes in the under-resolved case are slightly less pronounced than in the resolved case. In this two-species case, the two AP schemes seem to behave similarly as regards the energy dissipation properties and the lower energy dissipation of PICAP-2 compared with PICAP-1 is less apparent.
These results confirm that, in a situation where standard PIC methods would be unstable, the PICAP schemes remain stable and dissipate the electric energy of the plasma waves.

4.2 One-dimensional plasma expansion test-case

4.2.1 Setting of the problem

The second test-case we consider is that of a one-dimensional plasma expansion problem which is described in [22, 23]. This is a two-species problem where the ions initially occupy a slab of thickness L, while the electrons are initialized by a Maxwell-Boltzmann equilibrium with a self-consistent potential. The test problem consists in observing the expansion of the ion slab.
The initial electron temperature is 1000 times higher than the initial ion temperature. The simulation box is $[0, A]$ and the ions are initialized in $[0, L/2]$ with $L/2 \ll A$ (for reasons of symmetry, only half of the domain is simulated and a symmetry axis is set at $x = 0$). The mass ratio is $\varepsilon = 1/1836$. We scale the energies according to the electron thermal energy, using $\bar{\phi} = e\phi/(k_B T_{e0})$, $v_0 = k_B T_{e0}/m_i$ in (2.4). The scaled Vlasov-Poisson system is the same as before: (2.5)-(2.7). The boundary conditions for the potential are

$$\phi(0) = 0, \quad \partial_x \phi(A) = 0. \tag{4.4}$$

To enforce that $x = 0$ is an axis of symmetry, we assume specular reflection for the distribution function (i.e. particles are reinjected with reversed velocities), while the right boundary is a purely absorbing one, i.e. particles exiting the domain at $x = A$ are free to leave it while no particle is reinjected.
The initial electron density is defined by the Boltzmann relation

$$n_{e0} = n_0 \exp \phi_0, \tag{4.5}$$

while the initial ion density is such that

$$n_{i0} = \begin{cases} n_0 & \text{for} \quad 0 \le x \le L/2, \\ 0 & \text{for} \quad L/2 \le x \le A. \end{cases} \tag{4.6}$$

The initial potential ϕ_0 is obtained by solving the nonlinear Poisson equation (2.7) associated with the initial electron and ion densities (4.5), (4.6) and with the boundary conditions (4.4). The distribution functions are initialized by

$$f_{e0} = n_{e0} M_e(v), \quad f_{i0}(x, v) = n_{i0} M_i(v), \tag{4.7}$$

where the electron and ion Maxwellians are given by

$$M_e(v) = (\varepsilon/(2\pi))^{1/2} \exp(-\varepsilon v^2/2), \quad M_i(v) = (2\pi\eta)^{-1/2} \exp(-v^2/(2\eta)), \tag{4.8}$$

and $\eta = T_{i0}/T_{e0}$ is the ion to electron temperature ratio. In this test problem, $\eta = 10^{-3}$, and $L/2 = 20\lambda$.

In [23], the numerical parameters are chosen as follows. The simulation domain length is $A = 3 \times 10^4 \lambda$. The space step is $\Delta x = 0.2\lambda$ and there are 4×10^5 particles per cell. This makes a total number of 6×10^{10} particles, which exceeds our own computer resources. For this reason, we use a smaller simulation domain $A = 10^3 \lambda$ with the same $\Delta x = 0.2\lambda$ and 2000 particles per cell (1000 electrons and 1000 ions), which amounts to about 5×10^6 particles in total.

Because the domain is smaller, the Neumann boundary condition (4.4) at $x = A$ perturbs the resolution of the Poisson equation. Indeed, this condition being applied closer to the origin, the magnitude of the potential gradient inside the domain is reduced and the potential decays less for large x. Additionally, the smaller number of particles reduces the influence of the electrons for large x (because there are statistically very few of them there) which contributes to a slower decay of the electric potential as well. As a consequence, the expansion of the ion slab is slower than in [23]. Still, qualitatively, the features of our results are very similar to those of [23]. Because of this excellent agreement, and because the differences can be clearly attributed to the different choices of numerical parameters, we will assume that the classical PIC method with resolved time and space discretizations provides the reference solution and we will focus on comparing it to the PICAP method.

4.2.2 Simulation 1: time and space resolved case (reference case)

We first use the same time step as [23] i.e. $\Delta t = 0.05\omega^{-1}$, where $\omega = 1/(\sqrt{\varepsilon}\lambda)$ is the electron plasma frequency and we view the results at time $T = 30\omega_i^{-1}$ where $\omega_i = \sqrt{\varepsilon}\omega$ is the ion plasma frequency. These time and space steps obviously resolve the plasma period and Debye length.
The electric potential and electric field are shown on Fig. 9 and should be compared with Fig. 9 (a) and (b) of [23]. We observe that the boundary of the ion slab is located at $\sim 100\lambda$ instead of $\sim 140\lambda$ as in [23]. This location corresponds to the electric field peak which is created by the dipole layer due to the excess of positive ions on the left-hand side and the excess of negative electrons on the right-hand side of the layer. Both the classical PIC and the two PICAP methods yield identical results. This shows that this slower ion expansion is not specific of our method but simply depends on the choice of the numerical data, for the reasons explained above.
We note that the values reached by the two electric field peaks, close to the center of the foil ($E \sim 0.01E_0$) and at the boundary of the ion slab ($E \sim 0.03E_0$), measured in units of $E_0 = (n_0 k_B T/\varepsilon_0)^{1/2}$ are in very good agreement with [23]. The ion density distribution is shown on Fig. 10 (left) and the electron velocity distribution, on Fig. 10 (right). They must be compared respectively with Figs. 10 (a) and Fig. 3 (a) of [23]. Note that we display the space-integrated velocity distribution function rather than the distribution function at $x = 0$ as in [23] because otherwise, there are too few particles to make a significant statistics. The ion and electron mean velocities are shown in Fig. 11 and should be compared with Fig. 10 (b) of [23]. The ion density and velocity show an excellent agreement with [23] except for the location of the slab boundary and for the maximal velocity reached by the ions at the slab boundary, which is lower in our simulation, for the reasons detailed above. The electron velocity distribution also shows similar features as in [23]: a flat top, then a steep gradient between 0.25 and 0.5 in units of $2v_0^2$ and then an abrupt change to a flatter gradient around 0.5. The electron mean velocities are quite noisy due to the lack of significant statistics in the region beyond the boundary of the ion slab. This large noise level is also apparent in [23].

4.2.3 Simulation 2: time-resolved and space under-resolved case

We now perform simulations with a resolved time step and an under-resolved space step. Because of the huge velocities which are generated by the large electric fields, we cannot perform time under-resolved simulations while keeping the space-step as small as before. Indeed, this would otherwise violate the CFL condition (a given particle should not cross more than one cell per time step). Therefore, we select a significantly larger space-step, namely $\Delta x = 4\lambda$, but we keep the total particle number identical. In order to examine the influence of this larger space-step, we first run the simulations with the same resolved time-step as before, namely $\Delta t = 0.05\omega^{-1}$. The results are displayed in Figs. 12 to 15.

The electric potentials computed with the PICAP-1 and PICAP-2 methods (Fig. 12) are comparable to those of the reference simulation. The electric potential computed with the classical PIC method (Fig. 12) shows an exceedingly large slope which is clearly the signature of a mild instability. However, both computations exhibit a slope rupture at a position $x \sim 80\lambda$, which is slightly smaller than the value $x \sim 100\lambda$ which was found in the reference simulation (Fig. 9). This difference is confirmed on the figures showing the electric fields (Fig. 13). For both the classical PIC and PICAP methods, the electric field peak is located at $x \sim 80\lambda$, while the value found in the reference simulation is $x \sim 100\lambda$. This difference is due to a loss of accuracy resulting from the use of a larger space step. Obviously, this loss of accuracy manifests itself in the same manner for the classical PIC and PICAP methods, and cannot be attributed specifically to either method. We also notice that the electric field profiles provided by the PICAP methods (Fig. 13, right) are closer to the reference solution than the one obtained by the classical PIC method (Fig. 13, left). With the latter, the peak value is too high, and the profile close to the origin is wrong, probably because the Debye length in this region is very small and consequently, the space-step larger (relative to the Debye length), resulting in a stronger instability. By contrast, the electric field profiles provided by the PICAP methods are quite correct.

The slower slab expansion is also clearly visible on the ion density profiles on Fig. 14 (left). The boundary of the ion slab is located at $x \sim 87\lambda$. Again, both the classical PIC and PICAP methods exhibit a slower expansion, which can be attributed to the loss of accuracy resulting from the use of a larger space-step. In particular, there is no reason to assign this slower expansion to the use of the PICAP method. The electron distribution function profiles are

shown on Fig. 14 (right). Again, the PICAP methods provide fairly accurate results by comparison to the reference solution. The mild instability of the classical PIC method in this case is clearly visible on the incorrectly large number of fast velocity particles. The ion and electron mean velocities are displayed on Fig. 15. Both show quite good agreement with the fully resolved case except for the lower values of the peak velocities, which is consistent with the slower slab expansion.

4.2.4 Simulation 3: time and space under-resolved case

We now turn to fully under-resolved (in both time and space) simulations. To this aim, the space-step is kept to the value $\Delta x = 4\lambda$, but the time step is now chosen to be equal to $\Delta t = 3\omega^{-1}$. We present the electric potential and electric field on Figures 16 and 17. We observe that the classical PIC method gives nonsense: the electric potential is almost flat and the electric field is subject to large random fluctuations which have nothing to do with the expected solution. The PICAP methods on the other hand give fairly good agreements with the reference solution. We still observe the same qualitative features as in the resolved case, with a peak electric field located at the boundary of the ion slab, and a smaller but distinct peak close to the center of the foil. On the other hand, the magnitude of the electric field in the large x region (in the outer region to the ion slab) is reduced compared to the reference simulation. As a result, the ion expansion is further slowed down: the boundary of the ion slab is located at $x \sim 70\lambda$ and $x \sim 74\lambda$ for the PICAP-1 and PICAP-2 methods respectively as can be seen on the the ion density profiles on Fig. 18 (left). This further reduction of the ion expansion can again be attributed to the lower precision of the method due to the large time and space steps (Δt is 60 times bigger than in the reference case, while Δx is 20 times bigger). As we have noticed on the simulation with under-resolved space but resolved time steps, this loss of accuracy affects both the classical PIC and PICAP methods in the same way and cannot be attributed to the choice of the PICAP scheme. On the other hand, despite this slight degradation of accuracy, the PICAP methods provide fairly good results even in highly under-resolved situations, while the classical PIC method fails completely. The use of much larger time and space steps leads to a considerable speed-up of the numerical simulation over fully-resolved classical PIC simulations which makes the PICAP methods attractive compromises between accuracy and computational efficiency.

The ion density as a function of position (in log scale) and the electron velocity distribution as a function of $v^2/(2v_0^2)$ obtained in these under-resolved conditions are shown on Fig. 18 (left and right respectively). Again, apart from the slower expansion of the slab, the ion density profiles given by the PICAP methods are quite good, with a sharp decrease at the boarder of the slab, while the classical PIC method gives an almost uniform ion density, indicating that the ion slab has totally dissolved. We note that the PICAP-2 method seems slightly more accurate than the PICAP-1 method, as the ion expansion is faster with the former than with the latter. The main features of the electron velocity distribution are also quite well reproduced by the PICAP methods. The classical PIC method on the other hand shows an excess of large velocity particles. The ion and electron mean velocities are shown on Fig. 19. With the PICAP methods, the general trend of the ion mean velocity is preserved. The maximal ion velocity (attained at the boundary of the ion slab) is smaller than in the reference case, which is again consistent with the slower expansion of the ion slab.

4.2.5 Simulation 4: time and space under-resolved with small number of particles

These simulations show that the PICAP methods are able to produce fairly accurate results at much lower cost than the classical PIC method. To emphasize this point, we now show simulation results using much less particles. Specifically, using the same under-resolved time and space steps, we now initialize the simulation with 1000 particles per mesh for each species, like in the reference simulation. Since the mesh size is 20 times bigger than in the reference simulation, there are 20 times less particles, namely a total of about 2.5×10^5 particles. The results are displayed in Figs. 20 to 22. The electric potential and electric field show almost no difference with the previous simulation using 20 times more particles (see Figs. 16 and 17). The boundary of the ion slab as appearing on the density profiles in Fig. 21 (left), is located at the same position as in Fig. 18 (left). This indicates that the speed of the ion expansion is not affected by the number of particles. Because of the smaller number of particles, the statistics of the electron distribution function as appearing on Fig. 21 (right) degrades at large velocities. However, for low velocities, the results are similar to the previous case (see Fig. 18 (right)). The ion and electron mean velocities (Fig. 22) are also very similar to Fig. 19. The use of much larger time and space steps, together with a much smaller

number of particles, results in considerably faster simulations. Of course, the price to pay is a slight degradation of accuracy. However, it appears that the PICAP method provides an interesting compromise between accuracy and computational efficiency.

4.2.6 Computational speed-up and improvements

To illustrate this statement, we now compare the CPU time necessary to achieve the same final time step, using the time and space resolved classical PIC method on the one hand (Simulation 1), and the time and space under-resolved PICAP method on the other hand (Simulations 3 and 4). Table 1 displays the results. We normalize the CPU time to units of length and time equal to λ and ω^{-1} respectively and to one particle. Usually, the CPU time is normalized by the time and length steps but since the goal of the PICAP method is to use large time and space steps, we rather normalize the CPU time to the physical reference units.
The computational speed-up which can be obtained by the use of the PICAP method in the present situation is about 50 per particle. This means that Simulation 3, which uses the same number of particles as Simulation 1, is 50 times faster, but Simulation 4, which uses 20 times less particles, is about 1000 times faster. Given the extremely good qualitative agreement, this huge computationally speed-up can be extremely interesting for 2D and 3D simulations. Additionally, since the lower number of particles does not affect significantly the quality of the results, Simulation 4 also represents a considerable saving in terms of memory storage, which is also extremely interesting for higher dimensional simulations.
The degradation of accuracy related to the use of large time and space steps and small particle numbers seems to manifest itself in a slowing down of the time scales (such as that of the expansion of the ion slab). In general, in such circumstances, the method tends to overdamp the dynamics. However, the orders of magnitude are correct. These tests also showed that there is no significant difference between the two PICAP methods, apart from a slightly lower dissipation by the PICAP-2 method. Additionally, the PICAP-2 method being a one-step time advancement method, it is easier to implement and should be preferred over PICAP-1.
In order to further increase the computational speed-up, one needs to bypass the limitation given by the CFL condition, namely that any given particle should not move more than one mesh size per time step. We have tried

	Simulation 1 Classical PIC fully resolved	Simulation 3 or 4 PICAP fully under-resolved	Speed-up per particle PICAP/Class. PIC
CPU (sec) per particle, per λ, per ω^{-1}	$2.88\ 10^{-7}$	$6.0\ 10^{-9}$	48

Table 1: CPU Speed-up per particle. Note that a smaller number of particles can be used in conjunction with the PICAP method, thereby increasing the CPU speed-up (see text).

to loosen the CFL condition, but this rapidly leads to unacceptable errors. The reason is that the PICAP method is not asymptotic preserving with respect to the particle masses. Since the electron mass is the smallest, the CFL constraint is more restrictive for the electrons. Therefore, it would be extremely useful to design an asymptotic preserving PIC method associated with the small electron to ion mass ratio. Such a method is not available yet. A less efficient but probably easier method would be to use a local time-step and to take advantage of the less severe CFL constraint in the regions where the particle velocities are small. The use of a local space-step would also allow large cells in the regions of smooth gradients. In these regions, the CFL constraint could be locally loosened. Finally, the accuracy of the method could be increased by designing a second-order time integration method for the particle trajectories. All these research directions show that there exists a large potential of improvements for this method. These ideas will be implemented in future work.

5 Conclusion

In this paper, we have presented a novel PIC method for the Vlasov-Poisson equation. The method is Asymptotic Preserving in the quasineutral limit,

i.e. it is consistent with the quasineutral Vlasov equation in the limit of vanishing scaled Debye length. To validate this method, we have investigated two test problems: the first one consists of a perturbation of a quasi neutral plasma; the second one concerns the expansion of an ion slab in vacuum. Both tests have confirmed that the method is stable even if the time and space steps are well above the values set by the plasma period and Debye length, while the standard PIC method is unstable in these conditions. Despite the loss of accuracy associated with the use of large time and space steps, the method produces fairly accurate results and provides an attractive compromise between accuracy and computational efficiency. In the future, additional improvements of the method will be sought, such as for instance, removing the CFL constraint on the time step or finding second-order accurate time discretizations of the particle trajectories. The method will also be extended to electromagnetic plasma simulations through the coupling of the Vlasov equations to the Maxwell equations.

Acknowledgments

This work has been supported by the Marie Curie Actions of the European Commission in the frame of the DEASE project (MEST-CT-2005-021122) and by the french "Commissariat à l'Energie Atomique (CEA)" in the frame of the contract ASTRE "SAV 34-180". It has been conducted while the fourth author was visiting the "Institut de Mathématiques de Toulouse" in the academic year 2007-2008 under the auspices of the China Scholarship Council. The authors wish to express their gratitude to J. C. Adam for helpful discussions and suggestions.

References

[1] T. D. Arber, R. G. L. Vann, A critical comparison of eulerian-grid-based Vlasov solvers, J. Comput. Phys. 180 (2002) 339.

[2] R. Belaouar, N. Crouseilles, P. Degond, E. Sonnendrücker, An asymptotically stable semi-lagrangian scheme in the quasi-neutral limit, submitted.

[3] C. K. Birdsall, A. B. Langdon, Plasma physics via computer simulation, Taylor & Francis, 2004.

[4] J. U. Brackbill, D. W. Forslund, An implicit method for electromagnetic plasma simulation in two dimensions, J. Comput. Phys. 46 (1982) 271.

[5] Y. Brenier, Convergence of the Vlasov-Poisson system to the incompressible Euler equation, Comm. PDE, 25 (2000) 737.

[6] J. A. Carrillo, F. Vecil, Nonoscillatory interpolation methods applied to Vlasov-based models, SIAM J. Sci. Comput. 29 (2007) 1179.

[7] F. F. Chen, Introduction to plasma physics and controlled fusion, Plenum Press, 1974.

[8] B. I. Cohen, A. B. Langdon, A. Friedman, Implicit time integration for plasma simulation, J. Comput. Phys. 46 (1982) 15.

[9] G.-H. Cottet, P.-A. Raviart, Particle methods for the one-dimensional Vlasov-Poisson equations, SIAM J. Numer. Anal. 21 (1984) 52.

[10] P. Crispel, P. Degond, M.-H. Vignal, An asymptotically stable discretization for the Euler-Poisson system in the quasineutral limit, C. R. Acad. Sci. Paris, Ser.I, 341 (2005) 323.

[11] P. Crispel, P. Degond, M.-H. Vignal, Quasi-neutral fluid models for current-carrying plasmas, J. Comput. Phys. 205 (2005) 408.

[12] P. Crispel, P. Degond, M.-H. Vignal, An asymptotic preserving scheme for the two-fluid Euler-Poisson model in the quasineutral limit, J. Comput. Phys. 223 (2007) 204.

[13] P. Degond, F. Deluzet, L. Navoret, An asymptotically stable Particle-In-Cell (PIC) scheme for collisionless plasma simulations near quasineutrality, C. R. Acad. Sci. Paris, Ser.I, 343 (2006) 613.

[14] P. Degond, J. G. Liu, M.-H. Vignal, Analysis of an asymptotic preserving scheme for the Euler-Poisson system in the quasineutral limit, SIAM Num. Anal. 46 (2008) 1298.

[15] P. Degond, C. Parzani, M.-H. Vignal, Plasma expansion in vacuum: modeling the breakdown of quasineutrality, SIAM Multiscale Modeling and Simulation, 2 (2003) 158.

[16] F. Filbet, E. Sonnendrücker, Comparison of eulerian Vlasov solvers, Computer Physics Communications, 150 (2003) 247.

[17] A. Ghizzo, P. Bertrand, A Vlasov code for the numerical simulation of stimulated Raman scattering, J. Comput. Phys. 87 (1990) 495.

[18] A. Ghizzo, P. Bertrand, M. Shoucri, E. Fijalkow, M. R. Feix, An eulerian code for the study of the drift-kinetic Vlasov equation, J. Comput. Phys. 108 (1993) 105.

[19] K. Ganguly, H. D. Victory Jr. On the convergence of particles methods for multidimensional Vlasov-Poisson systems, SIAM J. Numer. Anal. 26 (1989) 249.

[20] F. Golse, L. Saint-Raymond, The Vlasov-Poisson system with strong magnetic field in quasineutral regime, Mathematical Models and Methods in Applied Sciences, 13 (2003) 661.

[21] E. Grenier, Defect measures of the Vlasov-Poisson system in the quasineutral regime, Comm. P.D.E. 20 (1995) 1189.

[22] T. Grismayer, Etude théorique et numérique de l'expansion d'un plasma créé par laser : accélération d'ions haute énergie, PhD dissertation, Ecole Polytechnique, Palaiseau, France, December 2006.

[23] T. Grismayer, P. Mora, J. C. Adam , A. Héron, Electron kinetic effects in plasma expansion and ion acceleration, Phys. Rev. E 77, 066407 (2008).

[24] S-Y. Ha, M. Slemrod, Global existence of plasma ion-sheaths and their dynamics, Comm. Math. Phys. 238 (2003) 149.

[25] D. W. Hewett, A. B. Langdon, Electromagnetic direct implicit plasma simulation, J. Comp. Phys. 72 (1987) 121.

[26] D. W. Hewett, C. W. Nielson, A Multidimensional Quasineutral Plasma Simulation Model, J. Comp. Phys. 29 (1978) 219.

[27] R. W. Hockney, J. W. Eastwood, Computer simulation using particles, Institute of Physics, 1988.

[28] S. Jin, Efficient Asymptotic-Preserving (AP) schemes for some multiscale kinetic equations, SIAM J. Sci. Comp. 21 (1999) 441.

[29] G. Joyce, M. Lampe, S. P. Slinker, W. M. Manheimer, Electrostatic Particle-in-Cell simulation technique for quasineutral plasma, J. Comp. Phys. 138 (1997) 540.

[30] N. A. Krall, A. W. Trivelpiece, Principles of plasma physics, San Francisco Press, 1986.

[31] A. B. Langdon, B. I. Cohen, A. Friedman, Direct implicit large time-step particle simulation of plasmas, J. Comp. Phys. 51 (1983) 107.

[32] A. B. Langdon, D. C. Barnes, Direct implicit plasma simulations, in: Multiple time scales, Academic Press, 1985.

[33] R. J. Mason, Implicit moment particle simulation of plasmas, J. Comp. Phys. 41 (1981) 233.

[34] R. J. Mason, Implicit moment PIC-hybrid simulation of collisional plasmas, J. Comp. Phys. 51 (1983) 484.

[35] R. J. Mason, Hybrid and collisional implicit plasma simulation models, in: Multiple time scales, Academic Press, 1985.

[36] R. J. Mason, An electromagnetic field algorithm for 2D implicit plasma simulation, J. Comp. Phys. 71 (1987) 429.

[37] Y.-J. Peng, Asymptotic limits of one-dimensional hydrodynamic models for plasma and semi-conductors, Chin. Ann. Math. B, 23 (2002) 25.

[38] E. Pohn, M. Shoucri, G. Kamelander, Eulerian Vlasov codes, Computer Physics Communications, 166 (2005) 81.

[39] P. W. Rambo, Finite-grid instability in quasineutral hydrid simulations, J. Comp. Phys. 118 (1995) 152.

[40] F. Valentini, P. Trávincek, F. Califano, P. Hellinger, A. Mangeney, A hybrid-Vlasov model based on the current advance method for the simulation of collisionless magnetized plasma, J. Comput. Phys. 225 (2007) 753.

[41] J. M. Wallace, J. U. Brackbill, D. W. Forslund, An implicit moment electromagnetic plasma simulation in cylindrical coordinates, J. Comp. Phys. 63 (1986) 434.

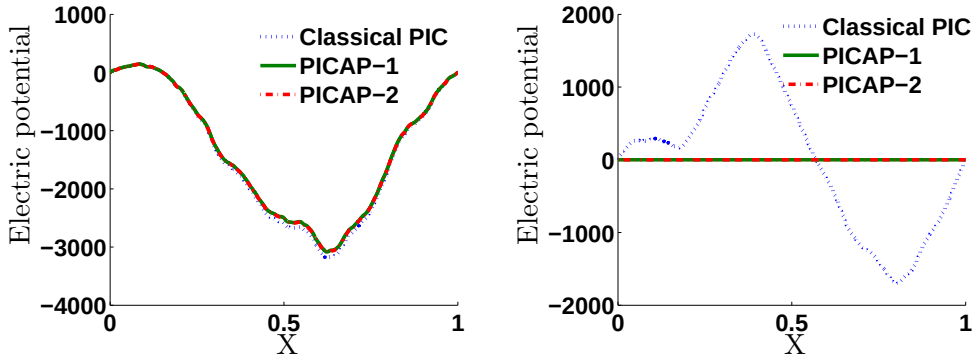

Figure 1: One-species periodic perturbation of a quasi-neutral Maxwellian plasma, resolved case: $\Delta x = \lambda = 10^{-4}$ and $\Delta t < \omega^{-1} = 10^{-4}$. Electric potential as a function of position, with Classical PIC, PICAP-1 and PICAP-2 schemes. Left: at scaled time $t = 10\omega^{-1} = 10^{-3}$ (all curves are identical) ; right: at scaled time $t = 0.2 = 2000\omega^{-1}$.

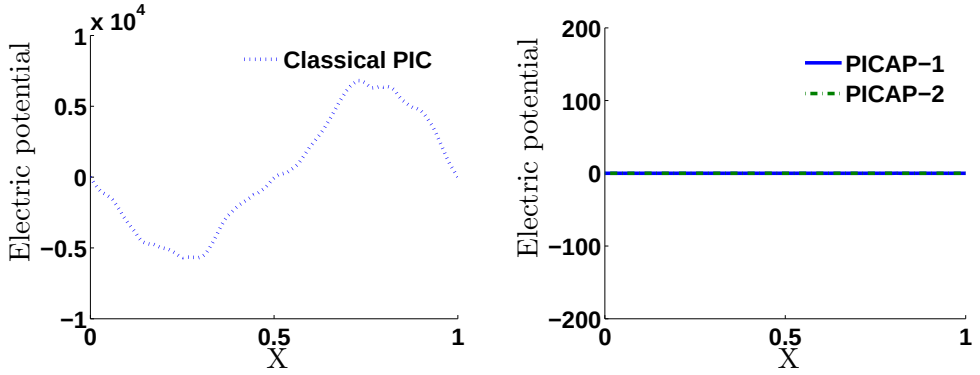

Figure 2: One-species periodic perturbation of a quasi-neutral Maxwellian plasma, under-resolved case: $\Delta x = 10^{-2} > \lambda = 10^{-4}$ and $\Delta t > \omega^{-1} = 10^{-4}$. Electric potential as a function of position, with Classical PIC scheme (left), and PICAP-1, PICAP-2 schemes (right), at scaled time $t = 0.2 = 2000\omega^{-1}$.

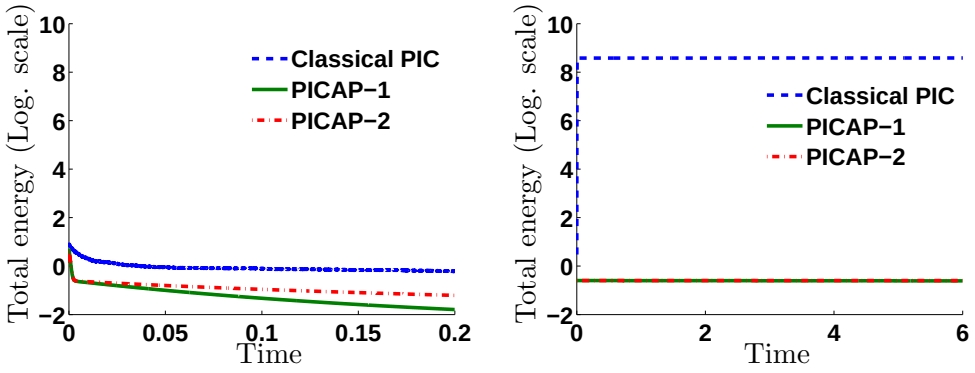

Figure 3: One-species periodic perturbation of a quasi-neutral Maxwellian plasma, with $\lambda = 10^{-4}$, $\omega = 10^4$: total energy in log scale as a function of scaled time, with Classical PIC, PICAP-1 and PICAP-2 schemes. Left: resolved case: $\Delta x = \lambda$ and $\Delta t < \omega^{-1}$; right: under-resolved case: $\Delta x = 10^{-2} > \lambda$ and $\Delta t > \omega^{-1}$.

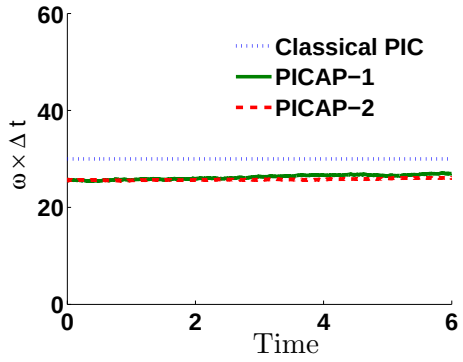

Figure 4: One-species periodic perturbation of a quasi-neutral Maxwellian plasma, under-resolved case: $\Delta x = 10^{-2} > \lambda = 10^{-4}$ and $\Delta t > \omega^{-1} = 10^{-4}$. $\omega \Delta t$ as a function of scaled time, with Classical PIC, PICAP-1 and PICAP-2 schemes.

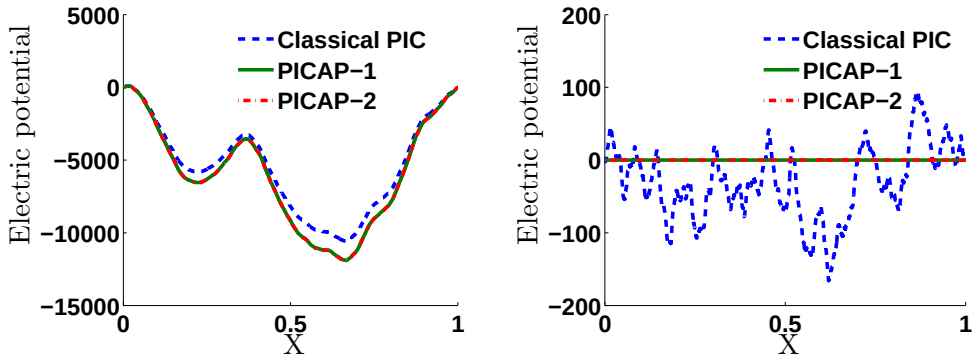

Figure 5: Two-species periodic perturbation of a quasi-neutral Maxwellian plasma, resolved case: $\Delta x = \lambda$ and $\Delta t < \omega^{-1}$ ($\Delta t = 0.9\Delta x/v_{max}$), $\varepsilon = 10^{-4}$, $\lambda = 10^{-4}$, $\omega = 10^6$. Electric potential as a function of position, with Classical PIC, PICAP-1 and PICAP-2 schemes. Left: scaled time $t = 3 \times 10^{-6} = 3\omega^{-1}$ (the curves corresponding to the PICAP-1 and PICAP-2 schemes are identical) ; right: scaled time $t = 8 \times 10^{-3} = 8000\omega^{-1}$.

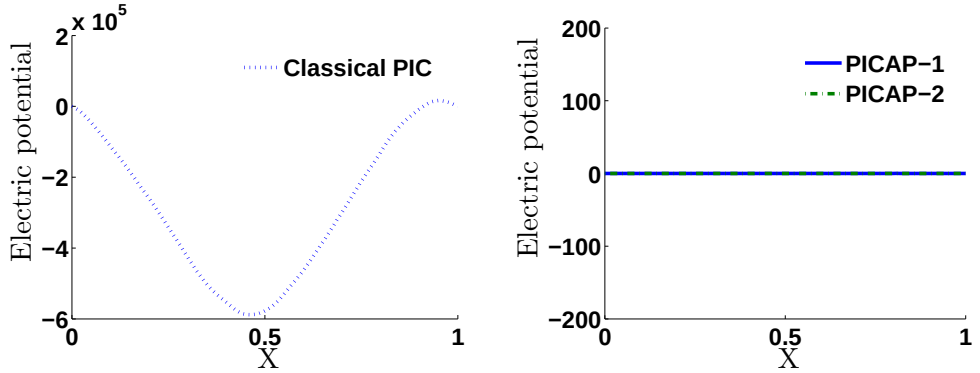

Figure 6: Two-species periodic perturbation of a quasi-neutral Maxwellian plasma, under-resolved case: $\Delta x = 10^{-2} > \lambda$ and $\Delta t > \omega^{-1}$ ($\Delta t = 0.9\Delta x/v_{max} \approx 25\omega^{-1}$), $\varepsilon = 10^{-4}$, $\lambda = 10^{-4}$, $\omega = 10^6$. Electric potential as a function of position, with Classical PIC (left), PICAP-1 and PICAP-2 schemes (right), at scaled time $t = 8 \times 10^{-3} = 8000\omega^{-1}$.

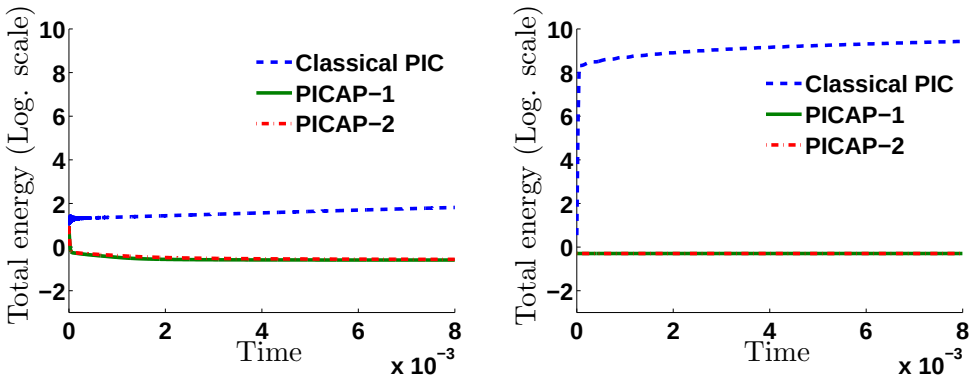

Figure 7: Two-species periodic perturbation of a quasi-neutral Maxwellian plasma, $\varepsilon = 10^{-4}$, $\lambda = 10^{-4}$, $\omega = 10^6$: total energy (in log scales) as a function of scaled time, with Classical PIC scheme, PICAP-1 and PICAP-2 schemes. Left: resolved case: $\Delta x = \lambda$ and $\Delta t < \omega^{-1}$ ($\Delta t = 0.9\Delta x/v_{max}$) ; right: under-resolved case: $\Delta x = 10^{-2} > \lambda$ and $\Delta t > \omega^{-1}$ ($\Delta t = 0.9\Delta x/v_{max} \approx 25\omega^{-1}$).

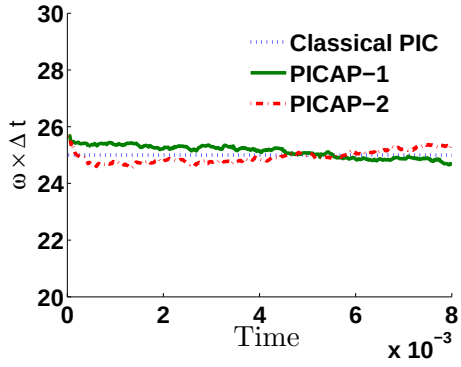

Figure 8: Two-species periodic perturbation of a quasi-neutral Maxwellian plasma, under-resolved case: $\Delta x = 10^{-2} > \lambda$ and $\Delta t > \omega^{-1}$, $\varepsilon = 10^{-4}$, $\lambda = 10^{-4}$, $\omega = 10^6$. $\omega\Delta t$ as a function of scaled time, with Classical PIC, PICAP-1 and PICAP-2 schemes.

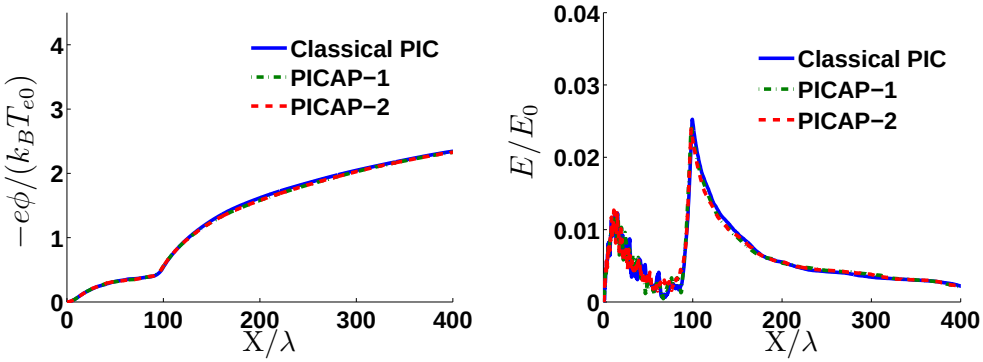

Figure 9: Plasma expansion test case. Simulation 1: resolved case (reference case): $\Delta x = 0.2\lambda$ and $\Delta t = 0.05\omega^{-1}$. Electric potential (left) and electric field (right) as functions of position, with Classical PIC, PICAP-1 and PICAP-2 schemes, at time $t = 30\omega_i^{-1}$. These pictures must be compared with Fig 9 (a) and (b) of reference [23].

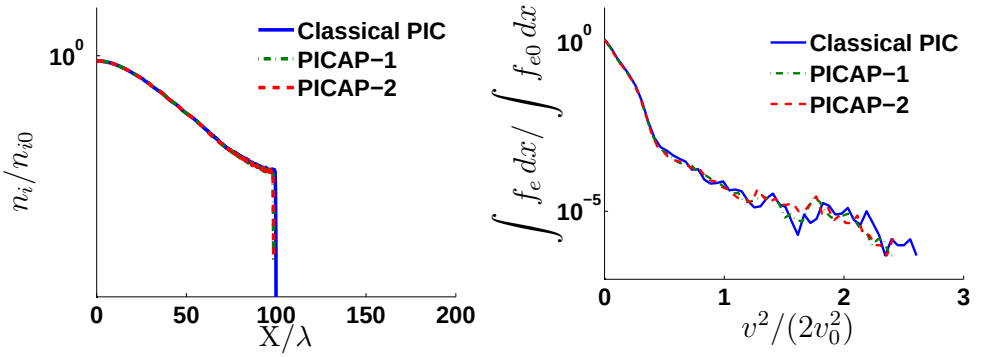

Figure 10: Plasma expansion test case. Simulation 1: resolved case (reference case): $\Delta x = 0.2\lambda$ and $\Delta t = 0.05\omega^{-1}$. Ion density as a function of position in log scale (left) and electron velocity distribution as a function of $v^2/(2v_0^2)$ (right) with Classical PIC, PICAP-1 and PICAP-2 schemes, at time $t = 30\omega_i^{-1}$. These pictures must be compared with Fig 10 (a) and Fig. 3 (a) (respectively) of reference [23].

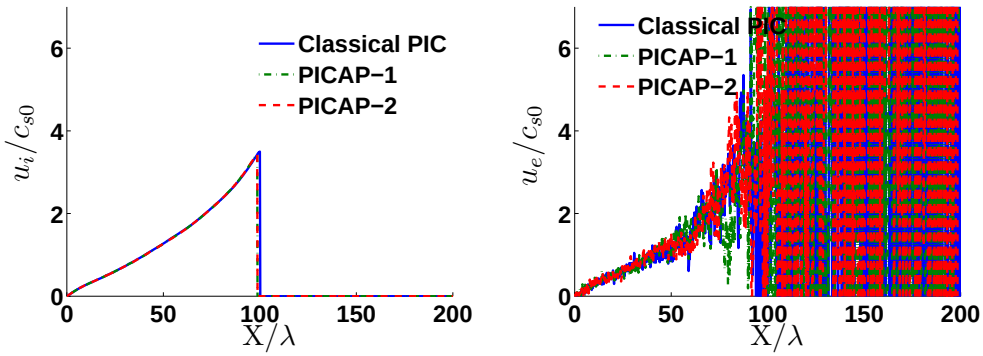

Figure 11: Plasma expansion test case. Simulation 1: resolved case (reference case): $\Delta x = 0.2\lambda$ and $\Delta t = 0.05\omega^{-1}$. Ion and electron mean velocities as functions of position, with Classical PIC, PICAP-1 and PICAP-2 schemes, at time $t = 30\omega_i^{-1}$ ($c_{s0} = \sqrt{k_B\, T_{e0}/m_i}$). These pictures must be compared with Fig 10 (b) of reference [23].

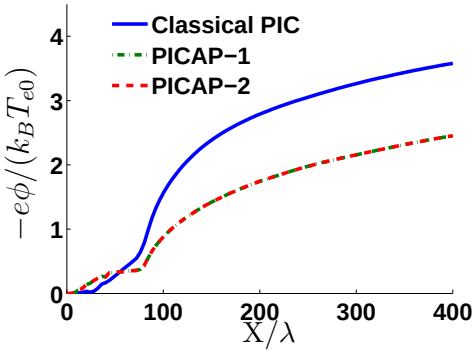

Figure 12: Plasma expansion test case. Simulation 2: space under-resolved and time resolved case: $\Delta x = 4\lambda$ and $\Delta t = 0.05\omega^{-1}$. Electric potential as a function of position, with Classical PIC scheme and PICAP schemes, at time $t = 30\omega_i^{-1}$.

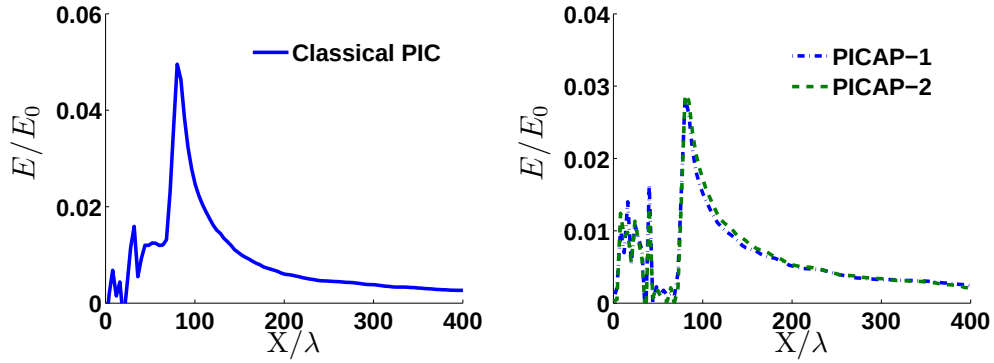

Figure 13: Plasma expansion test case. Simulation 2: space under-resolved and time resolved case: $\Delta x = 4\lambda$ and $\Delta t = 0.05\omega^{-1}$. Electric field as a function of position, with Classical PIC scheme (left) and PICAP schemes (right), at time $t = 30\omega_i^{-1}$.

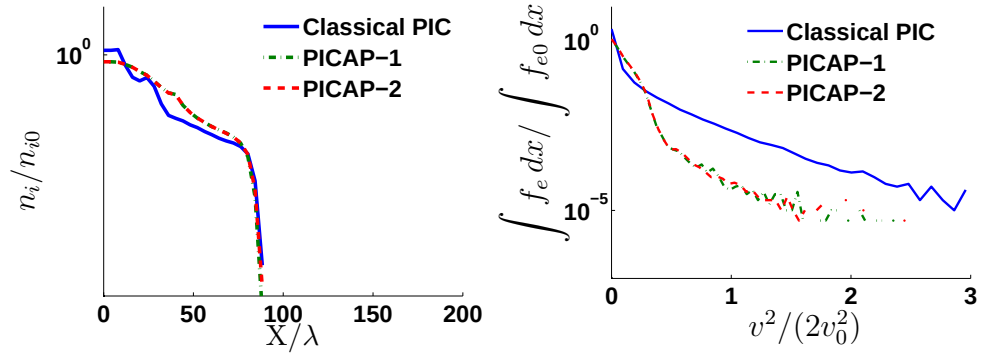

Figure 14: Plasma expansion test case. Simulation 2: space under-resolved and time resolved case: $\Delta x = 4\lambda$ and $\Delta t = 0.05\omega^{-1}$. Ion density as a function of position in log scale (left) and electron velocity distribution as a function of $v^2/(2v_0^2)$ (right) with Classical PIC and PICAP schemes, at time $t = 30\omega_i^{-1}$.

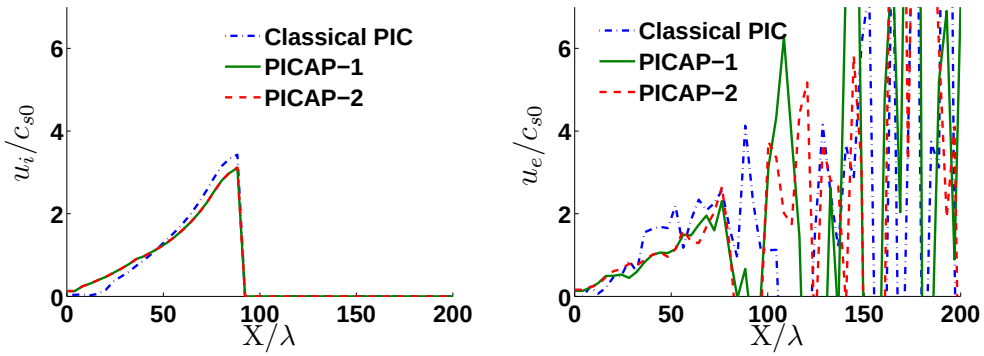

Figure 15: Plasma expansion test case. Simulation 2: space under-resolved and time resolved case: $\Delta x = 4\lambda$ and $\Delta t = 0.05\omega^{-1}$. Ion and Electron mean velocities as functions of position, with Classical PIC, PICAP-1 and PICAP-2 schemes, at time $t = 30\omega_i^{-1}$ ($c_{s0} = \sqrt{k_B\, T_{e0}/m_i}$).

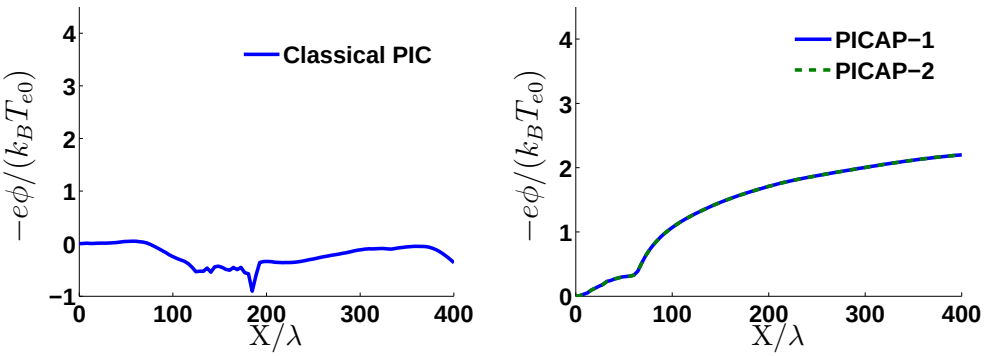

Figure 16: Plasma expansion test case. Simulation 3: space and time under-resolved case: $\Delta x = 4\lambda$ and $\Delta t = 3\omega^{-1}$. Electric potential as a function of position, with Classical PIC scheme (left) and PICAP schemes (right), at time $t = 30\omega_i^{-1}$.

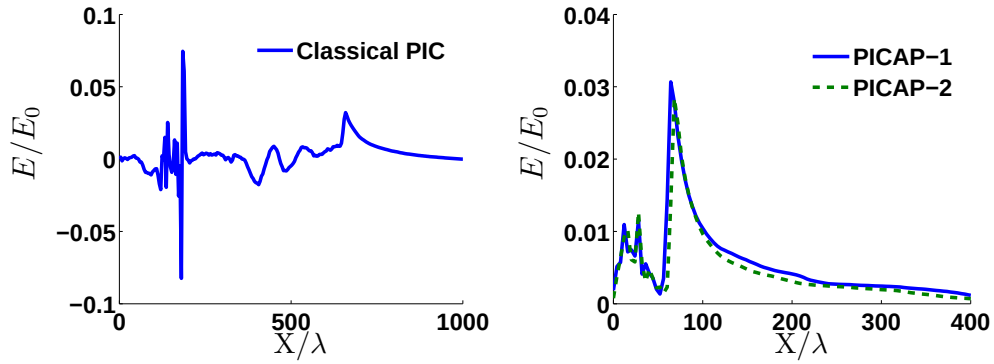

Figure 17: Plasma expansion test case. Simulation 3: space and time under-resolved case: $\Delta x = 4\lambda$ and $\Delta t = 3\omega^{-1}$. Electric field as a function of position, with Classical PIC scheme (left) and PICAP schemes (right), at time $t = 30\omega_i^{-1}$.

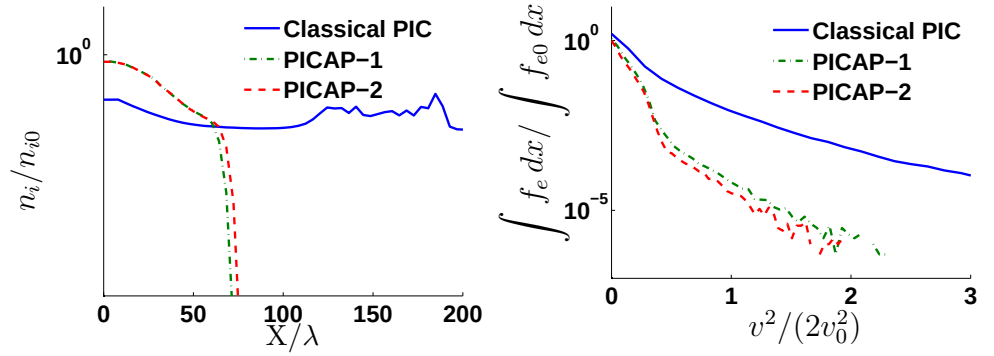

Figure 18: Plasma expansion test case. Simulation 3: space and time under-resolved case: $\Delta x = 4\lambda$ and $\Delta t = 3\omega^{-1}$. Ion density as a function of position in log scale (left) and electron velocity distribution as a function of $v^2/(2v_0^2)$ (right) with Classical PIC and PICAP schemes, at time $t = 30\omega_i^{-1}$.

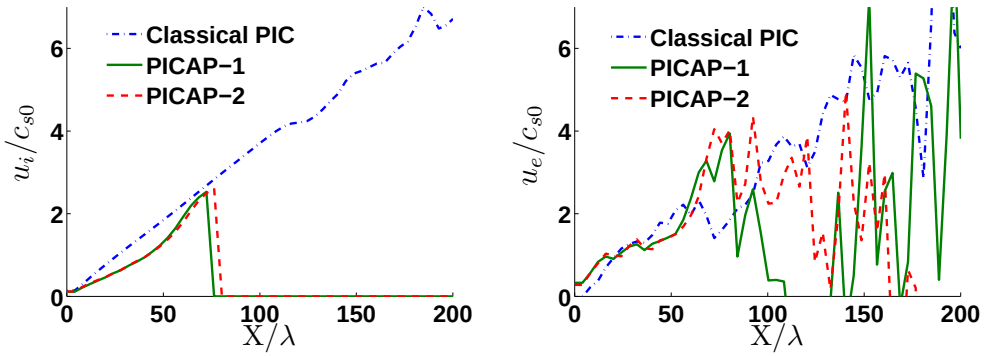

Figure 19: Plasma expansion test case. Simulation 3: space and time under-resolved case: $\Delta x = 4\lambda$ and $\Delta t = 3\omega^{-1}$. Ion and Electron mean velocities as functions of position, with Classical PIC, PICAP-1 and PICAP-2 schemes, at time $t = 30\omega_i^{-1}$ ($c_{s0} = \sqrt{k_B\, T_{e0}/m_i}$).

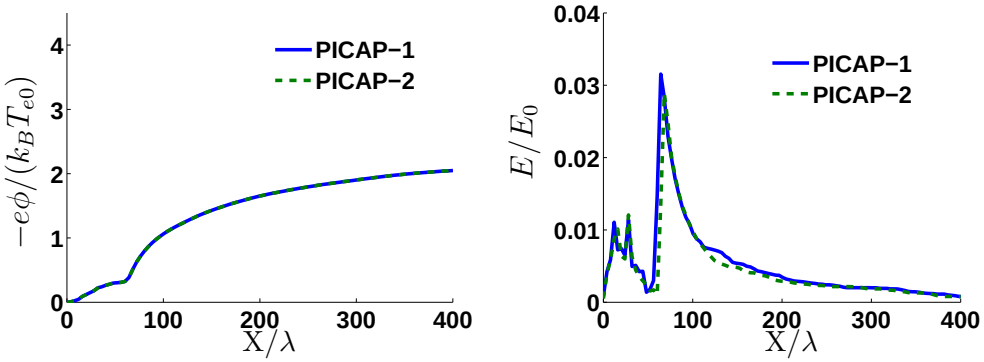

Figure 20: Plasma expansion test case. Simulation 4: space and time under-resolved case: $\Delta x = 4\lambda$ and $\Delta t = 3\omega^{-1}$ and small number of particles (1000 particles per mesh and per species). Electric potential (left) and electric field (right) as a function of position with PICAP schemes at time $t = 30\omega_i^{-1}$.

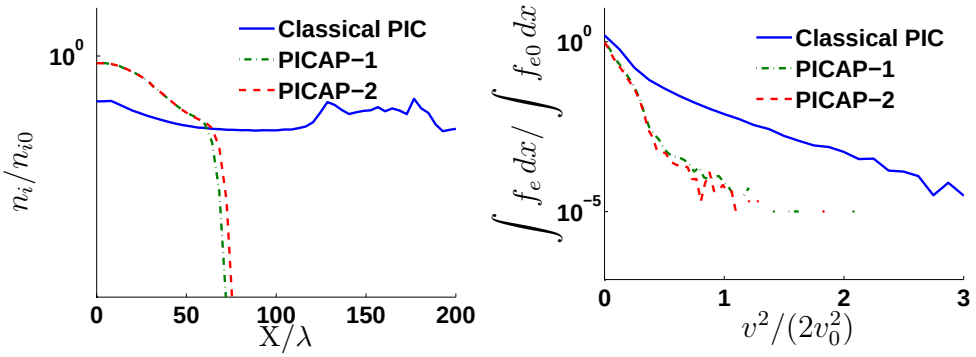

Figure 21: Plasma expansion test case. Simulation 4: space and time under-resolved case: $\Delta x = 4\lambda$ and $\Delta t = 3\omega^{-1}$ and small number of particles (1000 particles per mesh and per species). Ion density as a function of position in log scale (left) and electron velocity distribution as a function of $v^2/(2v_0^2)$ (right) with Classical PIC and PICAP schemes, at time $t = 30\omega_i^{-1}$.

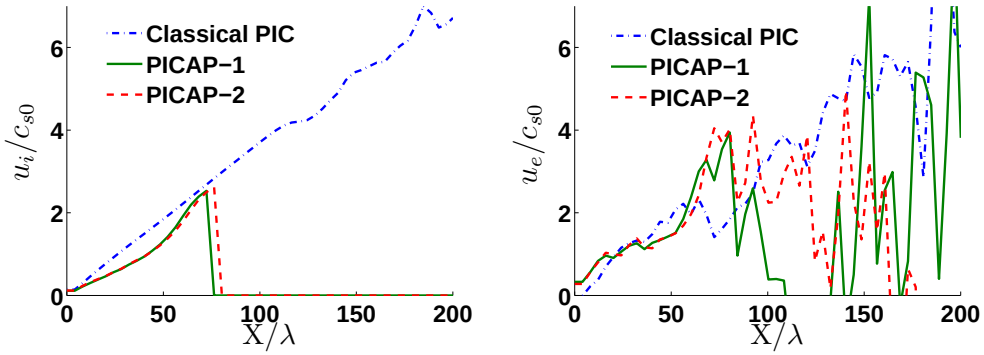

Figure 22: Plasma expansion test case. Simulation 4: space and time under-resolved case: $\Delta x = 4\lambda$ and $\Delta t = 3\omega^{-1}$ and small number of particles (1000 particles per mesh and per species). Ion and electron mean velocities as functions of position, with Classical PIC, PICAP-1 and PICAP-2 schemes, at time $t = 30\omega_i^{-1}$ ($c_{s0} = \sqrt{k_B\,T_{e0}/m_i}$).